ACS APPLIED MATERIALS & INTERFACES

Research Article

www.acsami.org

Ni_3S_2/Ni−P Bilayer Coated on Polyimide as a Pt- and TCO-Free Flexible Counter Electrode for Dye-Sensitized Solar Cells

Jeng-Yu Lin,* Wei-Yan Wang, Yi-Ting Lin, and Shu-Wei Chou

Department of Chemical Engineering, Tatung University, No. 40, Sec. 3, ChungShan North Road, Taipei City 104, Taiwan

Supporting Information

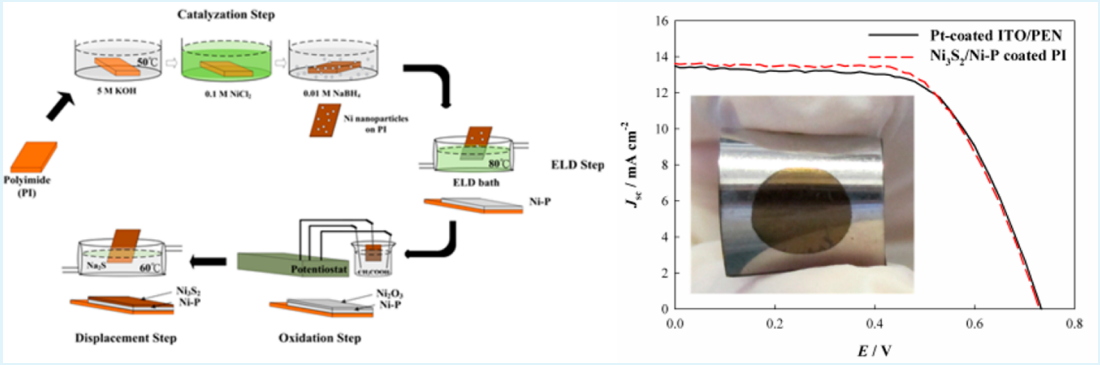

ABSTRACT: In this study, we reported an efficient, flexible, and low-cost (Pt-free and transparent conducting oxide (TCO)-free) counter electrode (CE) made of a polyimide (PI) substrate coated with a Ni_3S_2/Ni−P bilayer for dye-sensitized solar cells (DSCs). The bilayer Ni_3S_2/Ni−P hybrid film was deposited on a PI plastic substrate via a series of wet chemical/electrochemical processes. The bottom Ni−P layer was deposited on a PI to replace conventional TCO as a conductive layer, and the top Ni_3S_2 layer was employed as the electrocatalyst for I_3^- reduction. On the basis of the extensive electrochemical measurments, the as-prepared Ni_3S_2/Ni−P coated PI flexible CE demonstrated a Pt-like electrocatalytic for I_3^- reduction. As a result, the DSC assembled with the Ni_3S_2/Ni−P coated PI flexible CE exhibited an impressive photovoltaic conversion efficiency of 6.28% accompanied by a fill factor of 0.63 under 1 sun illumination (100 mW cm^{-2}, AM 1.5), which is comparative to that of the DSC based on the Pt coated indium tin oxide/polyethylene naphthalate (ITO/PEN) CE.

KEYWORDS: *Pt-free, TCO-free, flexible, bilayer, counter electrode, dye-sensitized solar cell*

1. INTRODUCTION

Dye-sensitized solar cells (DSCs) typically composed of a dye-sensitized nanocrystalline TiO_2 photoanode, an iodine-based redox electrolyte, and a counter electrode (CE) have attracted widespread attention as a promising candidate for next generation photovoltaics.[1,2] As a crucial component in DSCs, the essential functions of a CE are to promote the transfer of the electrons from the external circuit back to the redox electrolyte and speed up the reduction reaction from I_3^- to I^- in the electrolyte. As the most popular CE material, a Pt thin film coated on a transparent conducting oxide (TCO) such as indium tin oxide (ITO) or fluorine-doped tin oxide (FTO) has been demonstrated to show the high efficiency and long-term stability. However, due to the high price of TCO and noble Pt metal (more than 40% of the total cost),[3,4] the development of the Pt-free and TCO-free CEs is highly desirable.

To date, there are various types of Pt-free CE alternatives including carbon materials (graphite,[5] carbon nanotubes,[6,7] graphene,[8] etc.), conducting polymers (polyaniline,[9,10] poly(3,4-ethylene dioxythiophene) (PEDOT),[11,12] etc.), and inorganic compounds (transition metal in the form of oxides,[13] nitrides,[14] sulfides,[15−18] and carbides[19]). Although the aforementioned alternative CE materials show the comparable electrocatalytic activity to Pt metal, they are still deposited on the TCO layer as a current collector. Therefore, exploring totally TCO-free and Pt-free CEs for DSCs is still a huge challenge. Lee et al.[20] reported a highly conductive poly(3,4-ethylene dioxythiophene) (PEDOT) film on a glass substrate by using an in situ polymerization approach, and showed a comparable electrocatalytic activity toward the I_3^- reduction to the conventional Pt CE. Nagarajan et al.[21] have electroploymerized highly electrocatalytic PEDOT onto the conductive reinforced exfoliated graphite substrate, which exhibits an improved performance than the Pt CE. Therefore, it is anticipated that the combination of conductive TCO-free materials and highly electrocatalytic Pt-free catalysts provides a promising method for fabricating cost-effective CEs for DSCs.

In this paper, for the first time, we reported Ni_3S_2/Ni−P hybrid film coated on a polyimide (PI) substrate as a TCO-free and Pt-free flexible CE for DSCs. The bilayer Ni_3S_2/Ni−P

Received: November 26, 2013
Accepted: January 21, 2014
Published: January 21, 2014

   dx.doi.org/10.1021/am405384c | ACS Appl. Mater. Interfaces 2014, 6, 3357−3364

Scheme 1. Four-Step Chemical/Electrochemical Process of Ni_3S_2/Ni−P Bilayer Coated on PI Substrate

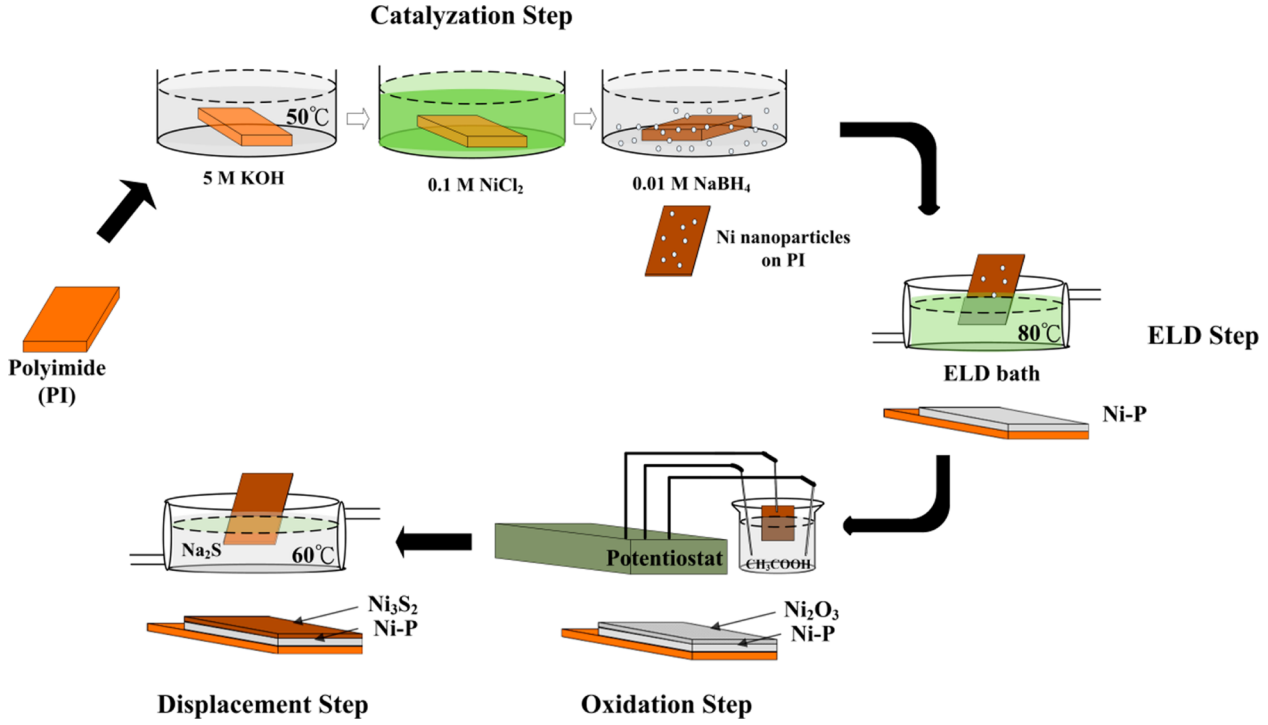

hybrid film was deposited on a PI plastic substrate via a series of chemical/electrochemical processes including the surface modification of PI substrate, ion exchange, activation, electroless deposition (ELD), oxidation, and displacement reaction. The bottom Ni−P layer replaces the conventional TCO as the conductive layer and the top Ni_3S_2 layer serves as the electrocatalyst for I_3^- reduction. Furthermore, PI was employed to replace conventional polyethylene naphthalate (PEN) and polyethylene terephthalate) as a flexible substrate due to its high thermal stability, excellent mechanical strength, and superior chemical resistance in acidic environments,[22,23] which can also facilitate the industrial roll-to-roll process. It is demonstrated that the DSC assembled with the Ni_3S_2/Ni−P coated PI CE achieved an impressive cell efficiency of 6.28%, comparable to that of the DSC using the Pt coated ITO/PEN CE (6.17%).

2. EXPERIMENTAL SECTION

2.1. Fabrication of CEs. Prior to the preparation, the PI films (50 μm, DuPont) were ultrasonically cleaned sequentially in ethanol and deionized water for 30 min, respectively. The preparation of the Ni_3S_2/Ni−P coated PI CE includes the following four steps, as illustrated in Scheme 1. In the first step (catalyzation step), the PI films were immersed into a 5 M KOH aqueous solution at 50 °C for 5 min. The alkaline aqueous solution reacted with the functional groups on the surface of PI substrate and thus a sublayer composed of potassium salts of poly(amic acid) was formed on the surface of PI substrate.[24] Then, the activation of the PI substrate was immersed into a 100 mM $NiCl_2$ (Acros) solution at 50 °C for 10 min, during which the doped K^+ ions within the sublayer were displaced by the Ni^{2+} ions via a facile ion exchange reaction. After immobilization, the PI substrate modified with the immobilized Ni^{2+} ions were rinsed with deionized water and immediately immersed into 0.01 M $NaBH_4$ aqueous solution for 1 h to reduce the immobilized Ni^{2+} ions in the form of Ni nanoparticles as catalysts for ELD of Ni−P.[25] Subsequently, the second step is the ELD of Ni−P on the modified PI substrate (ELD step), which was performed in the deposition bath (50 mL) consisting of 0.1 M $NiCl_2 \cdot 6H_2O$ (Acros), 0.25 M H_3BO_3 (Aldrich), 0.4 M lactic acid (Showa), and 0.25 M $NaPO_2 \cdot 6H_2O$ (Acros) at 70 °C for 3 min.[26] After the ELD of Ni−P layer, the surface of Ni−P coated PI film was further oxidized in an aqueous solution (50 mL) containing 0.1 M CH_3COOH (Aldrich) at pH 4 using a cyclic voltammetry method at a scan rate of 50 mV s^{-1} within the potential interval between −1 to +1 V vs saturated calomel electrode for 10 cycles (oxidation step). The Ni_3S_2/Ni−P coated PI film was subsequently obtained by soaking the resultant oxidized Ni−P coated PI film into an aqueous solution containing 5 mM $Na_2S \cdot 9H_2O$ at 60 °C for 5 min (displacement step). For comparison, ∼100 nm thick of Pt layer was sputtered on an ITO coated PEN substrate as a flexible Pt CE using a DC sputtering instrument (ULVAC) at a deposition rate of 0.28 nm s^{-1}.

2.2. Cell Assembly. First, a dense nanocrystalline TiO_2 film of about 8 μm thickness was loaded on the cleaned FTO glass from a commercial TiO_2 paste (ETERDSC Ti 2105, Eternal Chemical Co.) by using a semiautomatic screen printer (ATMA, AT45PA), followed by sintering under an air flow at 450 °C for 30 min. The screen-printable paste containing mesoporous TiO_2 beads was subsequently printed on the top of a dense nanocrystalline TiO_2 film as the scattering layer. Basically, the mesoporous TiO_2 beads were synthesized according to the previous studies.[27,28] In brief, amorphous precursor TiO_2 beads were initially prepared by introducing titanium(IV) isopropoxide (97%, Sigma-Aldrich) to an ethanol solution containing hexadecylamine (90%, Sigma-Aldrich) and 0.1 M KCl (Acros) aqueous solution under vigorous stirring at ambient atmosphere. The air-dried precursor beads were further dispersed in an ethanol−water mixture (2:1 by volume) containing 1.0 mL 25% ammonia aqueous solution. After that, the resulting mixture was sealed within a Teflon-lined autoclave and heated at 160 °C for 16 h. The mesoporous TiO_2 beads can be obtained by filtration, washed with ethanol, and dried at ambient atmosphere. After the construction of the scattering layer, the as-prepared TiO_2 photoanodes were sintered at 500 °C for 30 min. After being cooled to 80 °C, the sintered TiO_2 photoanodes were immersed into an ethanol solution containing 0.3 mM N719 dye (Everlight Chemical Industry Co.) and kept at 40 °C for 4 h. The dye-sensitized TiO_2 photoanode was assembled with a CE into a sandwich-type cell. After the injection of redox electrolyte, the sandwich-type cell was further sealed with a thermoplastic hot-melt Surlyn (30 μm thick, Dupont). The redox electrolyte was composed of

1 M 1.3-dimethylimidazolium iodine (Merck), 0.5 M 4-*tert*-butylpyridine (Aldrich), 0.15 M iodine (J.T. Baker), and 0.1 M guanidine thiocyanate (Aldrich) in 3-methoxypropionitrile (Acros) solvent.

2.3. Characterizations and Measurements. The chemical configurations of samples were determined using an automated grazing incident X-ray diffractometer (GIXRD, Rigaku D/TTRAX) and an X-ray photoelectron spectroscopy (XPS) with PHI Quantera SXM (ULVAC-PHI). The energy calibrations for the resultant XPS results were made against the C 1s peak to eliminate the charging of the sample during analyses. The surface morphology of the samples was characterized by a scanning electron microscopy (JSM-700F). High-resolution transmission electron microscope (HRTEM, JEOL JEM-2100F) equipped with an energy dispersive spectrometer (EDS) was further employed to obtain the information on the microstructures. The reflection spectra of the CEs were recorded using a UV/vis/NIR spectrometer (V-560, Jasco). The electrochemical measurements including CV, electrochemical impedance spectroscopy (EIS), and Tafel polarization measurements were conducted by means of a CHI614d potentiostat. The CV tests were performed at a scan rate of 10 mV s^{-1} in 3-methoxypropionitrile solution consisting of 50 mM LiI, 10 mM I_2, and 50 mM $LiClO_4$ in a three-electrode system, in which the as-fabricated CE acted as the working electrode, in addition to a Pt sheet (4 cm^2) counter electrode and a Pt wire reference electrode. The EIS and Tafel polarization measurements were carried out using the symmetric configuration cells with two identical CEs. The redox electrolyte for EIS and Tafel measurements was the same one used in the photovoltaic measurements. The EIS measurements were performed at the open circuit potential with ac amplitude of 5 mV over a frequency region of 0.1 Hz to 50 kHz. The resultant Nyquist plots were fitted by the software of ZSimpWin version 3.1. The cell performance of DSCs was measured under AM 1.5 illumination using a computer-controlled Keithley Model 2400 digital source meter, during which a solar simulator (Yamashita Denso YSS-150A) calibrated to 1 sun light density with a radiant power/energy meter (Oriel, 70260) was used as a light source.

3. RESULTS AND DISCUSSION

To characterize the chemical structures of the as-prepared thin films, GIXRD analyses were carried out. As shown in curve A of Figure 1, a single broad peak at ca. 45° is attributed to the characteristic of amorphous structure with preferred orientation of Ni (111) formed after the ELD process on a PI substrate according to the XRD pattern.[29,30] Several studies have reported that a broad peak with a width larger than 10° occurs as a result of the amorphous structure of supersaturated Ni–P film.[30,31] On the basis of the previous report, high content of P element in the Ni coating may cause lattice disorder in the crystalline Ni and therefore the structure becomes amorphous.[31,32] Moreover, EDX analysis (Figure S1a, Supporting Information) shows that the ELD Ni–P thin film contains ca. 15 wt % P and HRTEM analysis clearly proves the Ni–P thin film with an amorphous structure (Figure S1b, Supporting Information). Therefore, it is evident that the high content of P element can prevent the nucleation of f.c.c. Ni and result in the Ni–P thin film with an amorphous structure, which is consistence with the data from XRD study. It should be noted that others peaks are attributed to the signals from the PI substrate. Therefore, a Ni–P layer coated on a PI substrate (denoted as Ni–P coated PI CE) was made. After the oxidation of the Ni–P coated PI CE, the resultant spectrum (curve b of Figure 1) shows the similar diffraction peaks to those of the Ni–P coated PI CE. To further verity its chemical structure, XPS analysis of the oxidized Ni–P coated PI CE was carried out. Figure S2 (Supporting Information) shows the high resolution XPS spectra of Ni 2p and O 1s for the oxidized Ni–P coated PI CE. As seen in Figure S2a (Supporting Information), the Ni spectrum (including Ni $2p_{3/2}$ and Ni $2p_{1/2}$ peaks) consists of at least three constituents. Generally, the Ni $2p_{3/2}$ is composed of the satellite signals at high binding energy adjacent to the main peaks.[33] Due to the consideration of the satellite peaks, the Ni $2p_{3/2}$ peaks at binding energies of 852.3, 857.1, and 861.3 eV could be assigned to Ni, Ni_2O_3, and $Ni(CH_3COO)_2$. The presence of $Ni(CH_3COO)_2$ in the oxidized Ni–P coated PI CE may be possibly ascribed to the adsorption of the $Ni(CH_3COO)_2$ complexes on the Ni–P sublayer. The strong intensity of Ni signal can be attributed to the Ni–P sublayer. Figure S2b (Supporting Information) further illustrates the curve fitting of the O 1s spectrum of the oxidized Ni–P coated PI CE, the corresponding spectrum can be deconvoluted into two main peaks, Ni_2O_3 and P_2O_5.[34] These results reveal that the main composition of the oxidized ELD Ni–P layer could be Ni_2O_3 and the signature peaks of Ni_2O_3 may overlap with the peaks of Ni–P sublayer based on the corresponding XRD pattern (PDF #897390). After soaking the Ni_2O_3/Ni–P coated on a PI substrate (denoted as Ni_2O_3/Ni–P coated PI CE) in an aqueous consisting of 5 mM $Na_2S\cdot 9H_2O$ at 60 °C for 5 min (curve C), the peaks at 31.1°, 37.8°, 49.7°, and 55.2° are emerged, which can be attributed to the diffractions from (110), (111), (210), and (211) planes of the Rhombohedral Ni_3S_2 lattice. Thus, the Ni_3S_2/Ni–P layer coated on the PI substrate (denoted as Ni_3S_2/Ni–P coated PI) was successfully prepared.

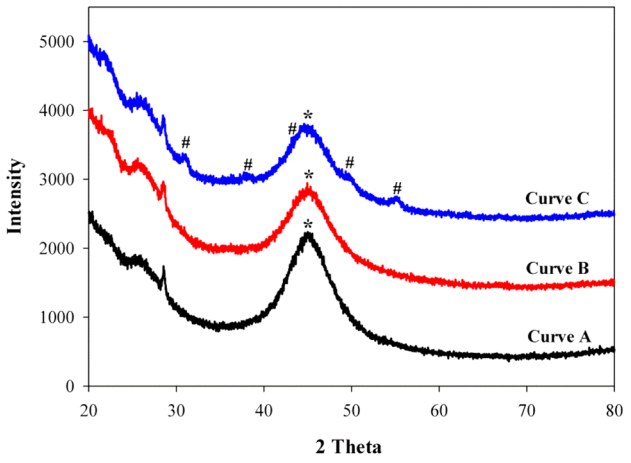

Figure 1. XRD patterns of the as-prepared Ni–P coated PI (curve A), Ni_2O_3/Ni–P coated PI (curve B), and Ni_3S_2/Ni–P coated PI (curve C). The * and # symbols correspond to the diffraction peaks for Ni and Ni_3S_2, respectively.

Figures 2 and 3 show the surface morphology and photographs of bare PI, Ni–P coated PI, Ni_2O_3/Ni–P coated PI, and Ni_3S_2/Ni–P coated PI CEs. Before the ELD Ni–P deposition, the flat and smooth surface can be observed for the PI substrate (Figure 2a). After the PI substrate was subjected to the ELD Ni–P deposition, the formation of a Ni–P layer generates the characteristic of metal lusteris (Figure 3a,b). It should be mentioned that the sheet resistance of Ni–P coated PI is only 5.12 Ω cm^{-2}, which is even lower than that of the ITO coated PEN substrate (15 Ω cm^{-2}). This result suggests the Ni–P layer is a proper material for charge collection.

Figure 2b reveals that the resultant Ni–P layer is composed of semispherical Ni–P particles. After the oxidation of the Ni–P coated PI CE, the semispherical morphology is broken up

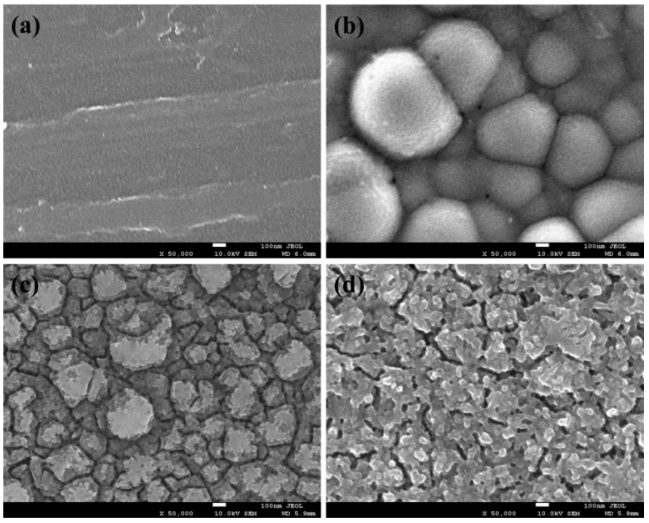

Figure 2. FESEM images of (a) bare PI, (b) Ni–P coated PI, (c) Ni_2O_3/Ni–P coated PI, and (d) Ni_3S_2/Ni–P coated PI CEs.

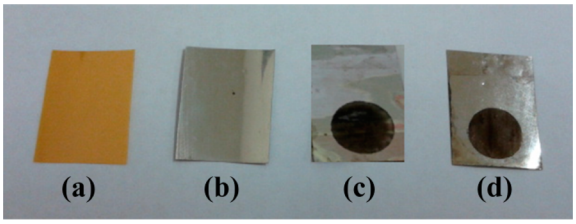

Figure 3. Photographs of (a) bare PI, (b) Ni–P coated PI, (c) Ni_2O_3/Ni–P coated PI, and (d) Ni_3S_2/Ni–P coated PI CEs.

and then a granular-like morphology is obtained. Moreover, the color of the thin film is apparently changed to dark brown (Figure 3c) due to the presence of Ni^{3+} ions in the Ni_2O_3 assignment, serving as color centers.[35] This result also confirms the observation from the XPS analyses. After Ni_2O_3 is converted into Ni_3S_2, the color of the deposit remains dark brown (Figure 3d) and the corresponding surface morphology becomes a mesoporous structure (Figure 2d). Furthermore, the pull-off adhesion test for the Ni_3S_2/Ni–P coated PI CE performed by using 3M flatback masking tape is illustrated in Figure S3 (Supporting Information). After the test, no deposit came off for the Ni_3S_2/Ni–P coated PI CE, indicating its good mechanical contact performance.

A series of CV experiments were conducted to compare the electrocatalytic activity of the various CEs in the I^-/I_3^- redox system, where the corresponding redox reactions can be expressed by eqs 1 and 2.[36,37]

$$3I^- \rightarrow I_3^- + 2e^- \text{ (anodic peak)} \quad (1)$$

$$I_3^- + 2e^- \rightarrow 3I^- \text{ (cathodic peak)} \quad (2)$$

Figure 4 shows the CVs curves of Pt coated ITO/PEN, Ni_2O_3/Ni–P coated PI, and Ni_3S_2/Ni–P coated PI CEs. Notably, no significant redox peaks can be observed for the Ni_2O_3/Ni–P coated PI CEs, signifying its poor electrocatalytic activity for the I_3^- reduction. When Ni_2O_3/Ni–P coated PI CE is converted into Ni_3S_2/Ni–P coated PI CE, the latter shows a similar redox peaks toward I_3^-/I^- redox reaction to the Pt coated ITO/PEN CE, pointing to its Pt-like electrocatalytic activity. Compared to the Pt coated ITO/PEN CE, the Ni_3S_2/Ni–P coated PI CE possesses higher cathodic current density.

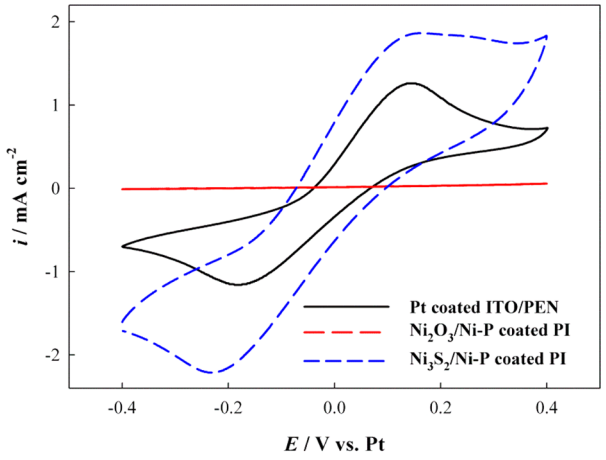

Figure 4. CVs of I_3^-/I^- redox couple for Pt coated ITO/PEN, Ni_2O_3/Ni–P coated PI, and Ni_3S_2/Ni–P coated PI CEs.

The cathodic current density is generally associated with the rate of reaction for I_3^- reduction. The enhanced i_{pc} value can be ascribed to its mesoporous structure, not only providing a relatively larger active surface area for I_3^- reduction but also constructing lots of open channels to facilitate the diffusion of I^-/I_3^- redox species.[38,39]

Figure 5a shows 50 consecutive CV scans of the Ni_3S_2/Ni–P coated PI CE. In the consecutive 50 CV tests, both of anodic and cathodic current densities are increased at the first 10 successive CV cycles. However, the shape of the CVs after 10 cycles does not change a lot. This can be ascribed to the fact that the electrolyte infiltrates into the Ni_3S_2/Ni–P coated PI CE completely until consecutive 10 CV cycles. The correlations between the redox peak current densities and the cycle numbers are also summarized in Figure 5b. Both redox peak current densities retain stable with increasing the cycle number after 10 CV cycles. This indicates that the Ni_3S_2/Ni–P coated PI CE has excellent chemical and electrochemical stability.

To elucidate the electrocatalytic kinetics for the CEs, the EIS measurements were conducted and the resultant Nyquist plots are illustrated in Figure 6.The Nyquist plots were fitted to the equivalent circuit model illustrated in Figure S4 (Supporting Information). The equivalent circuit model consists of a Randles-type circuit composed of a charge transfer resistance (R_{ct}) and a parallel double-layer capacitance (C_{dl}) plus a series resistance (R_s) and the Nernst diffusion resistance (Z_N). The obtained EIS parameters are summarized in Table 1. Generally, the low R_{ct} value at the CE/electrolyte interface indicates the low overpotential for the electron transfer from the CE to the I_3^- species.[36,37] It can be observed that the R_{ct} value for the Ni_2O_3/Ni–P coated PI CE is larger than 15 Ω cm^2, indicating its poor electrocatalytic activity as evidenced by the CV tests. For Ni_3S_2/Ni–P coated PI CE, the corresponding R_{ct} value is merely 1.95 Ω cm^2, which is comparable to that of the Pt coated ITO/PEN CE (2.51 Ω cm^2). This confirms that the Ni_3S_2/Ni–P coated PI CE possesses a Pt-like electrocatalytic activity for I_3^- reduction.

To get more insight into the electrocatalytic characteristics of the CEs, Tafel polarization measurements were performed. Figure 7 presents the Tafel polarization curves for the Pt coated ITO/PEN, Ni_2O_3/Ni–P coated PI, and Ni_3S_2/Ni–P coated PI CEs. The curves present logarithmic current density as a function of potential and thus the corresponding exchange current density (J_0) for each CE can be evaluated, as also listed

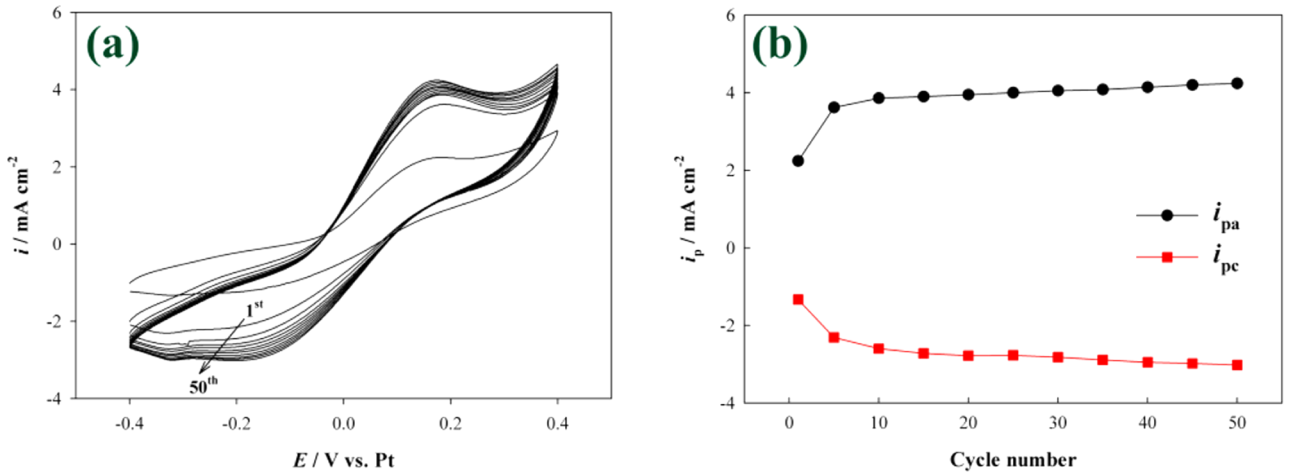

Figure 5. (a) A total of 50 consecutive CVs for the I_2/I^- system using the Ni_3S_2/Ni−P coated PI CE at a scan rate of 10 mV s^{-1}, (b) The relationship between the cycle time and the redox peak current for the Ni_3S_2/Ni−P coated PI CE. i_{pa} and i_{pc} represent the anodic and cathodic current densities, respectively.

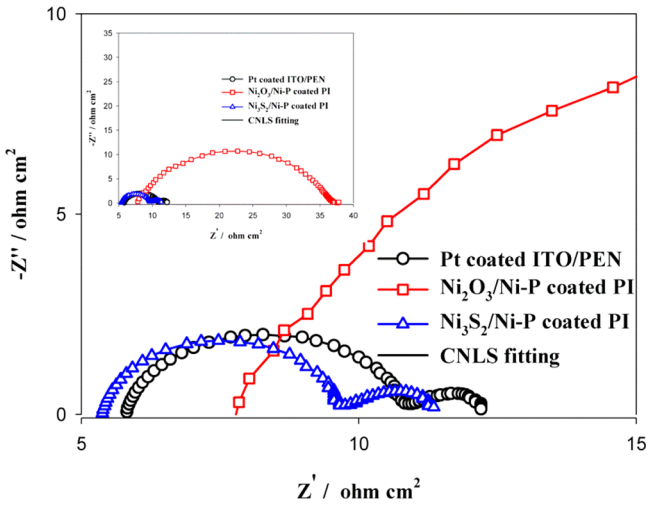

Figure 6. Nyquist plots of EIS for symmetric cells assembled with Pt coated ITO/PEN, Ni_2O_3/Ni−P coated PI, and Ni_3S_2/Ni−P coated PI CEs.

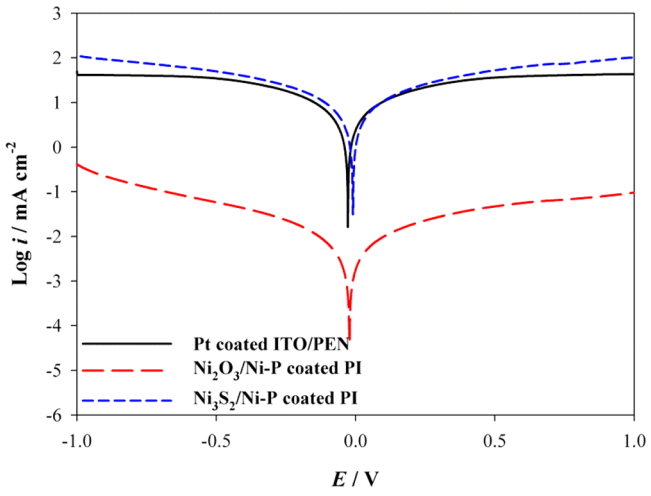

Figure 7. Tafel polarization curves of symmetric cells assembled with Pt coated ITO/PEN, Ni_2O_3/Ni−P coated PI, and Ni_3S_2/Ni−P coated PI CEs.

in Table 1. It is noteworthy that the significant enhancement in the J_0 value is observed when the Ni_2O_3/Ni−P coated PI CE is totally converted to the Ni_3S_2/Ni−P coated PI CE. Moreover, the Ni_3S_2/Ni−P coated PI CE has a comparable J_0 value to that of the Pt coated ITO/PEN CE, which is in a well accordance withthe R_{ct} values obtained from the EIS measurements in terms of eq 3.[40] Furthermore, the intersection of the cathodic branch with the *y*-axis can be regarded as the limiting current density (J_{lim}). It can be observed that Ni_3S_2/Ni−P coated PI CE has a relatively larger J_{lim} value than the Pt coated ITO/PEN CE. According to eq 4,[15] J_{lim} is positively relevant to the diffusion coefficient (D), which corresponds to the diffusion behavior of the I^-/I_3^- redox couple in the electrolyte. There, the diffusion coefficients of the I_3^- species for the Ni_3S_2/Ni−P coated PI and Pt coated ITO/PEN CEs were estimated to be 1.55×10^{-5} cm^2 s^{-1} and 2.17×10^{-5} cm^2 s^{-1}, respectively. The improved diffusion behavior in the Ni_3S_2/Ni−P coated PI CE may be ascribed to the fact that lots of open channels can be constructed for the transport of redox species due to its mesoporous structure, as suggested by the CV results.

$$J_0 = \frac{RT}{nFR_{ct}} \quad (3)$$

$$D = \frac{l}{2nFC}J_{lim} \quad (4)$$

Table 1. Electrochemical and Photovoltaic Parameters for Different CEs

CEs	σ (Ω sq^{-1})	R_s ($\Omega \cdot cm^2$)	R_{ct} ($\Omega \cdot cm^2$)	J_0 ($mA \cdot cm^{-2}$)	J_{sc} ($mA \cdot cm^{-2}$)	V_{oc} (mV)	FF	η (%)
Pt coated ITO/PEN	1.05	5.36	2.51	3.33	13.36	733	0.63	6.17
Ni_2O_3/Ni−P coated PI	19.91	7.75	15.62	0.25	5.37	708	0.23	0.86
Ni_3S_2/Ni−P coated PI	10.59	5.66	1.95	3.42	13.62	729	0.63	6.28

dx.doi.org/10.1021/am405384c | ACS Appl. Mater. Interfaces 2014, 6, 3357−3364

where R represents the gas constant, T is the temperature, F is the Faraday constant, n is the number of electrons exchanged in the reaction at the CE/electrolyte interface, D is the diffusion coefficient of the I_3^- species, l is the spacer thickness, and C is the concentration of I_3^- species.

Figure 8 shows the photovoltaic performance of DSCs with various CEs measured under the illumination of 1 sun (100 mW cm^{-2}). The resultant photovoltaic parameters are also summarized in Table 1. As expected, the DSC with the Ni_2O_3/Ni−P coated PI CE exhibits a poor cell efficiency of 0.86% due to its poor electrocatalytic activity. The DSC based on the Ni_3S_2/Ni−P coated PI CE has an open-circuit voltage (V_{oc}) of 729 mV, a short-circuit current (J_{sc}) of 13.62 mA cm^{-2}, and a fill factor (FF) of 0.63, thus resulting in an impressive cell efficiency (η) of 6.28%. Compared to the DSC assembled with the Ni_2O_3/Ni−P coated PI CE, the DSC based on the Ni_3S_2/Ni−P coated PI CE shows the remarkable improvement in FF and J_{sc} values, resulting in that the photovoltaic performance of the Ni_3S_2/Ni−P coated PI based DSC is comparable to that of the Pt coated ITO/PEN based DSC (6.17%). It can be observed that the V_{oc} and FF of the DSCs based on the Ni_3S_2/Ni−P coated PI and Pt coated ITO/PEN CEs are similar. In general, the V_{oc} value of a DSC is determined by the difference between the Fermi level for electrons in the photoanode and the redox potential of I^-/I_3^-. Due to the no change in the photoanodes and the redox electrolyte in this study, V_{oc} values of the DSCs based on Ni_3S_2/Ni−P coated PI and Pt coated ITO/PEN CEs remain almost the same. As for the FF, it is mainly determined by the internal resistance of the device.[5] Although the Ni_3S_2/Ni−P coated PI CE possesses a relatively lower R_{ct} than that of Pt coated ITO/PEN CE, the Pt coated ITO/PEN CE is with lower R_s value due to its lower sheet resistance of 1.05 Ω sq^{-1} compared to the Ni_3S_2/Ni−P coated PI CE (5.12 Ω sq^{-1}) as shown in Table 1. These two factors counterbalance each other, thus resulting in the similar FF values for the DSCs based on these two CEs. It should be noted that the increased active surface area of a CE generally promotes the electrocatalytic activity for I_3^- reduction and thus increases the total current of the I^-/I_3^- redox reaction. This could enhance the photogenerated electron transport at the CE/redox electrolyte interface and thus an enhanced J_{sc} value can be expected.[16,36] Therefore, the improved J_{sc} value for the Ni_3S_2/Ni−P coated PI based DSC can be ascribed to its mesoporous structure. Moreover, the improved FF can also result from the enhanced electrocatalytic activity of Ni_3S_2/Ni−P coated PI CE with low R_{ct} of 1.95 Ω cm^2.[41,42] According to CV results (Figure 3), the J_{sc} value for the DSC with the Ni_3S_2/Ni−P coated PI CE should be much higher than that of the DSC with the Pt coated ITO/PEN CE. Nevertheless, the Ni_3S_2/Ni−P coated PI based DSC only demonstrates a slightly higher J_{sc} value than that of DSC using the Pt coated ITO/PEN CE. It can be attributed to the fact that the high reflectivity of the mirror-like sputtered Pt is expected to reflect the unabsorbed portion of incident solar light back to the TiO_2 photoanode, thus enhancing the light-harvesting efficiency of the DSCs.[43] However, this effect is almost completely obstructed for the opaque Ni_3S_2/Ni−P coated PI CE (Figure S5, Supporting Information).

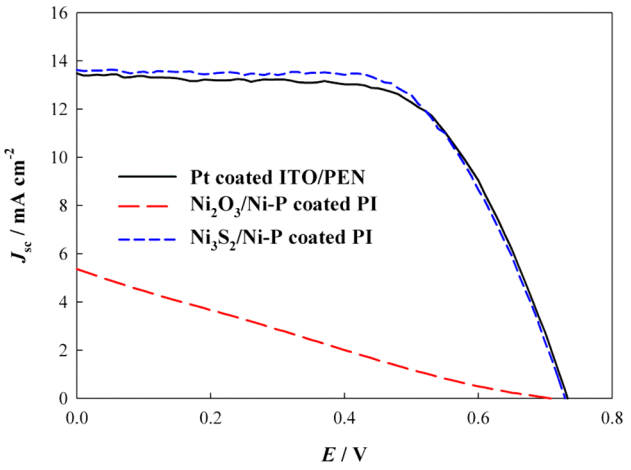

Figure 8. Photovoltaic characteristics of DSCs assembled with Pt coated ITO/PEN, Ni_2O_3/Ni−P coated PI, and Ni_3S_2/Ni−P coated PI CEs.

4. CONCLUSIONS

In summary, we have successfully prepared a Pt- and TCO-free flexible CE made of a PI film coated with a Ni_3S_2/Ni−P bilayer for low-cost DSCs via a series of facile wet chemical/electrochemical processes for the first time. According to the extensive electrochemical analyses, the as-prepared Ni_3S_2/Ni−P coated PI flexible CE demonstrated a Pt-like electrocatalytic for I_3^- reduction due to the synergistic effect of the high electrocatalytic activity of Ni_3S_2 and facile electron transport of the conductive Ni−P layer. The DSC assembled with the Ni_3S_2/Ni−P coated PI flexible CE achieved an impressive photovoltaic conversion efficiency of 6.28%, which is comparable to that based on the Pt CE. In addition, the proposed chemical/electrochemical processes have the features of facile, continuous and low-temperature, and thus make it applicable to large-scale flexible substrates.

■ ASSOCIATED CONTENT

Ⓢ Supporting Information

The EDS spectrum and HRTEM image of Ni−P coated PI CE, the XPS spectra of Ni_3S_2/Ni−P coated PI flexible CE, the equivalent circuits used for fitting the EIS results, the pull-off adhesion test for the Ni_3S_2/Ni−P coated PI CE, and the reflection spectra of Pt coated ITO/PEN and Ni_3S_2/Ni−P coated PI CEs. This material is available free of charge via the Internet at http://pubs.acs.org.

■ AUTHOR INFORMATION

Corresponding Author

*J.-Y. Lin. E-mail: jylin@ttu.edu.tw. Fax: +886-225861939.

Notes

The authors declare no competing financial interest.

■ ACKNOWLEDGMENTS

This research was supported by National Science Council Taiwan (NSC 102-2221-E-036-034).

■ REFERENCES

(1) O'Regan, B.; Grätzel, M. A low-cost, high-efficiency solar cell based on dye-sensitized colloidal TiO_2 films. *Nature* **1991**, *353*, 737−740.

(2) Grätzel, M. Photoelectrochemical cells. *Nature* **2001**, *414*, 338−344.

(3) Smestad, G.; Bignozzi, C.; Argazzi, R. Testing of dye sensitized TiO_2 solar cells I: Experimental photocurrent output and conversion efficiencies. *Sol. Energy Mater. Sol. Cells* **1994**, *32*, 259−272.

(4) Chen, J.; Li, K.; Luo, Y.; Guo, X.; Li, D.; Deng, M.; Huang, S.; Meng, Q. A flexible carbon counter electrode for dye-sensitized solar cells. *Carbon* **2009**, *47*, 2704−2708.
(5) Veerappan, G.; Bojan, K.; Rhee, S. W. Sub-micrometer-sized Graphite As a Conducting and Catalytic Counter Electrode for Dye-sensitized Solar Cells. *ACS Appl. Mater. Interfaces* **2011**, *3*, 857−862.
(6) Malara, F.; Manca, M.; Marco, L. D.; Pareo, P.; Gigli, G. Flexible Carbon Nanotube-Based Composite Plates As Efficient Monolithic Counter Electrodes for Dye Solar Cells. *ACS Appl. Mater. Interfaces* **2011**, *3*, 3625−3632.
(7) Lin, J. Y.; Lien, C. H.; Chou, S. W. Multi-wall carbon nanotube counter electrodes for dye-sensitized solar cells prepared by electrophoretic deposition. *J. Solid State Electrochem.* **2012**, *16*, 1415−1421.
(8) Yen, M. Y.; Hsien, C. K.; Teng, C. C.; Hsiao, M. C.; Liu, P. I.; Ma, C. C. M.; Tsai, M. C.; Tsai, C. H.; Lin, Y. R.; Chou, T. Y. Metal-free, nitrogen-doped graphene used as a novel catalyst for dye-sensitized solar cell counter electrodes. *RSC Adv.* **2012**, *2*, 2725−2728.
(9) Li, Q. H.; Wu, J. H.; Tang, Q. W.; Lan, Z.; Li, P. J.; Lin, J. M.; Fan, L. Q. Application of microporous polyaniline counter electrode for dye-sensitized solar cells. *Electrochem. Commun.* **2008**, *10*, 1299−1302.
(10) Xiao, Y.; Lin, J. Y.; Wang, W. Y.; Tai, S. Y.; Yue, G.; Wu, J. Enhanced performance of low-cost dye-sensitized solar cells with pulse-electropolymerized polyaniline counter electrodes. *Electrochim. Acta* **2013**, *90*, 468−474.
(11) Pringle, J. M.; Armel, V.; MacFarlane, D. R. Electrodeposited PEDOT-on-plastic cathodes for dye-sensitized solar cells. *Chem. Commun.* **2010**, *46*, 5367−5369.
(12) Xiao, Y.; Lin, J. Y.; Wu, J.; Tai, S. Y.; Yue, G. Pulse potentiostatic electropolymerization of high performance PEDOT counter electrodes for Pt-free dye-sensitized solar cells. *Electrochim. Acta* **2012**, *83*, 221−226.
(13) Wu, M. X.; Lin, X.; Hagfeldt, A.; Ma, T. L. A novel catalyst of WO_2 nanorod for the counter electrode of dye-sensitized solar cells. *Chem. Commun.* **2011**, *47*, 4535−4537.
(14) Li, G. R.; Song, J.; Pan, G. L.; Gao, X. P. Highly Pt-like electrocatalytic activity of transition metal nitrides for dye-sensitized solar cells. *Energy Environ. Sci.* **2011**, *4*, 1680−1683.
(15) Wang, M. K.; Anghel, A. M.; Marsan, B.; Ha, N. C.; Pootrakulchote, N.; Zakeeruddin, S. M.; Grätzel, M. CoS Supersedes Pt as Efficient Electrocatalyst for Triiodide Reduction in Dye-Sensitized Solar Cells. *J. Am. Chem. Soc.* **2009**, *131*, 15976−15977.
(16) Lin, J. Y.; Liao, J. H.; Chou, S. W. Cathodic electrodeposition of highly porous cobalt sulfide counter electrodes for dye-sensitized solar cells. *Electrochim. Acta* **2011**, *56*, 8818−8826.
(17) Sun, H. C.; Qin, D.; Huang, S. Q.; Guo, X. Z.; Li, D. M.; Luo, Y. H.; Meng, Q. B. Dye-sensitized solar cells with NiS counter electrodes electrodeposited by a potential reversal technique. *Energy Environ. Sci.* **2011**, *4*, 2630−2637.
(18) Chi, W. S.; Han, J. W.; Yang, S.; Roh, D. K.; Lee, H.; Kim, J. H. Employing electrostatic self-assembly of tailored nickel sulfide nanoparticles for quasi-solid-state dye-sensitized solar cells with Pt-free counter electrodes. *Chem. Commun.* **2012**, *48*, 9501−9503.
(19) Jang, J. S.; Ham, D. J.; Ramasamy, E.; Lee, J.; Lee, L. S. Platinum-free tungsten carbides as an efficient counter electrode for dye sensitized solar cells. *Chem. Commun.* **2010**, *46*, 8600−8602.
(20) Lee, K. S.; Lee, H. K.; Wang, D. H.; Park, N. G.; Lee, J. Y.; Park, O. O.; Park, J. H. Dye-sensitized solar cells with Pt- and TCO-free counter electrodes. *Chem. Commun.* **2010**, *46*, 4505−4507.
(21) Nagarajan, S.; Sudhagar, P.; Raman, V.; Cho, W.; Dhathathreyan, K. S.; Kang, Y. S. A PEDOT-reinforced exfoliated graphite composite as a Pt- and TCO-free flexible counter electrode for polymer electrolyte dye-sensitized solar cells. *J. Mater. Chem. A* **2013**, *1*, 1048−1054.
(22) Ma, T.; Fang, X.; Akiyama, M.; Inoue, K.; Noma, H.; Abe, E. Properties of several types of novel counter electrodes for dye-sensitized solar cells. *J. Electroanal. Chem.* **2004**, *574*, 77−83.
(23) Dow, W. P.; Liao, G. L.; Huang, S. E.; Chen, S. W. Modification of Cu nanoparticles with a disulfide for polyimide metallization. *J. Mater. Chem.* **2010**, *20*, 3600−3609.
(24) Akamatsu, K.; Shinkai, H.; Ikeda, S.; Adachi, S.; Nawafune, H.; Tomita, S. Controlling Interparticle Spacing among Metal Nanoparticles through Metal-Catalyzed Decomposition of Surrounding Polymer Matrix. *J. Am. Chem. Soc.* **2005**, *127*, 7980−7981.
(25) Hsiao, Y. S.; Whang, W. T.; Wu, S. C.; Chung, K. R. Chemical formation of palladium-free surface-nickelized polyimide film for flexible electronics. *Thin Solid Films* **2008**, *516*, 4258−4266.
(26) Wang, G.; Lin, R.; Lin, Y.; Li, X.; Zhou, X.; Xiao, X. A novel high-performance counter electrode for dye-sensitized solar cell. *Electrochim. Acta* **2005**, *50*, 5546−5552.
(27) Chen, D. H.; Cao, L.; Huang, F. Z.; Imperia, P.; Cheng, Y. B.; Cheng; Caruso, R. A. Synthesis of Monodisperse Mesoporous Titania Beads with Controllable Diameter, High Surface Areas, and Variable Pore Diameters (14−23 nm). *J. Am. Chem. Soc.* **2010**, *132*, 4438−4444.
(28) Lin, J. Y.; Lin, Y. T. Electroless platinum counter electrodes with Pt-activated self-assembled monolayer on transparent conducting oxide. *Surf. Coat. Technol.* **2012**, *206*, 4672−4678.
(29) Mahallawy, N. E.; Bakkar, A.; Shoeib, M.; Palkowski, H.; Neubert, V. Electroless Ni−P coating of different magnesium alloys. *Surf. Coat. Technol.* **2008**, *202*, 5151−5157.
(30) Aal, A. A.; Hassan, H. B.; Rahim, M. A. A. Nanostructured Ni−P−TiO_2 composite coatings for electrocatalytic oxidation of small organic molecules. *J. Electroanal. Chem.* **2008**, *619−620*, 17−25.
(31) Ashassi-Sorkhabi, H.; Rafizadeh, S. H. Effect of coating time and heat treatment on structures and corrosion characteristics of electroless Ni−P alloy deposits. *Surf. Coat. Technol.* **2004**, *176*, 318−326.
(32) Lin, J. Y.; Lin, C. Y.; Liu, S. K.; Wan, C. C.; Wang, Y. Y. Characterization of electroless Ni-based alloys for use in bipolar plates of direct methanol fuel cells. *Surf. Coat. Technol.* **2010**, *205*, 2251−2255.
(33) Casella, I. G.; Guascito, M. R.; Sannazzaro, M. G. Voltammetric and XPS investigations of nickel hydroxide electrochemically dispersed on gold surface electrodes. *J. Electroanal. Chem.* **1999**, *462*, 202−210.
(34) Moulder, J. F.; Stickle, W. F.; Sobol, P. E.; Bomben, K. D. *Handbook of X-ray Photoelectron Spectroscopy*, 1st ed.; Chastain, J., King, R. C., Eds.; Physical Electronics Division, Perkin-Elmer Corp.: Eden Prairie, MN, 1995; p 231.
(35) Kitao, M.; Izawa, K.; Urabe, K.; Komatsu, T.; Kuwano, S.; Yamada, S. Preparation and Electrochromic Properties of RF-Sputtered NiO_x Films Prepared in $Ar/O_2/H_2$ Atmosphere. *Jpn. J. Appl. Phys.* **1994**, *33*, 6656−6662.
(36) Tai, S. Y.; Liu, C. J.; Chou, S. W.; Chien, F. S. S.; Lin, J. Y.; Lin, T. W. Few-layer MoS_2 nanosheets coated onto multi-walled carbon nanotubes as a low-cost and highly electrocatalytic counter electrode for dye-sensitized solar cells. *J. Mater. Chem.* **2012**, *22*, 24753−24759.
(37) Lin, J. Y.; Chan, C. Y.; Chou, S. W. Electrophoretic deposition of transparent MoS_2−graphene nanosheet composite films as counter electrodes in dye-sensitized solar cells. *Chem. Commun.* **2013**, *49*, 1440−1442.
(38) Lin, J. Y.; Liao, J. H. Mesoporous Electrodeposited-CoS Film as a Counter Electrode Catalyst in Dye-Sensitized Solar Cells. *J. Electrochem. Soc.* **2012**, *159*, D65−D71.
(39) Sudhagar, P.; Nagarajan, S.; Lee, Y. G.; Song, D.; Son, T.; Cho, W.; Heo, M.; Lee, K.; Won, J.; Kang, Y. S. Synergistic Catalytic Effect of a Composite (CoS/PEDOT:PSS) Counter Electrode on Triiodide Reduction in Dye-Sensitized Solar Cells. *ACS Appl. Mater. Interfaces* **2011**, *3*, 1838−1843.
(40) Bard, A. J.; Faulkner, L. R. *Electrochemical Methods: Fundamentals and Applications*; 2nd ed.; John Wiley & Sons: New York, 1980, p 115.
(41) Kaven, L.; Yum, J. H.; Grätzel, M. Optically Transparent Cathode for Dye-Sensitized Solar Cells Based on Graphene Nanoplatelets. *ACS Nano* **2011**, *5*, 165−172.

(42) Jeon, S S.; Kim, C.; Ko, J.; Im, S. S. Pt Nanoparticles Supported on Polypyrrole Nanospheres as a Catalytic Counter Electrode for Dye-Sensitized Solar Cells. *J. Phys. Chem. C* **2011**, *115*, 22035−22039.
(43) Fang, X.; Ma, T.; Guan, G.; Akiyama, M.; Kida, T.; Abe, E. Effect of the thickness of the Pt film coated on a counter electrode on the performance of a dye-sensitized solar cell. *J. Electroanal. Chem.* **2004**, *570*, 257−263.